A Comparative Study of Conventional Single-Mass and Amplitude Amplified Dual-Mass MEMS Vibratory Gyroscopes

Danmeng Wang, Mohammad H. Asadian, Alexandra Efimovskaya, Andrei M. Shkel
MicroSystems Laboratory
University of California, Irvine, CA 92697, USA
Email: {danmenw, asadianm, aefimovs, ashkel}@uci.edu

***Abstract*—This paper presents preliminary experimental results on a novel dual-mass MEMS gyroscope with mechanical amplification of amplitude. A side-by-side comparison between proposed dual-mass and conventional single-mass gyroscopes is presented and the effect of amplitude amplification on the scale factor and noise characteristics is discussed. The dual-mass gyroscope demonstrated a scale factor of 0.465 mV/(deg/s) in the open-loop rate-mode of operation, which is three times higher sensitivity than the single-mass gyroscope. The dual-mass gyroscope also showed a superior performance in bias stability and Angle Random Walk (ARW).**

Keywords*—MEMS gyroscopes; amplitude amplification; dual-mass gyroscope

I. Introduction

MEMS Coriolis Vibratory Gyroscopes (CVGs) are classified into two main categories: rate gyroscopes, which measure the angular velocity, and rate-integrating (or whole angle) gyroscopes, which measure the angle of rotation, [1]. The large sensing amplitude for both operational modes is projected to improve signal-to-noise ratio and to increase sensitivity. However, the large amplitude in capacitive MEMS devices would result in non-linearity of parallel plate actuation. To address the challenge, we investigate a dual-mass architecture, which mechanically couples an outer mass to a single-mass structure and can operate as a vibratory gyroscope in both rate and rate-integrating modes. When the ratios of masses and stiffnesses are selected correctly, the design allows for an amplification in the amplitude of motion of the outer mass. The outer mass, or "sense mass", would follow the linearly actuated inner mass, or "drive mass", and would respond with an amplified amplitude, thus offering a potential mitigation of the small amplitude challenge. The concept of amplitude amplification and a dual-mass architecture were introduced previously in [2] and [3].

To demonstrate advantages of the amplitude amplified device, we designed a dual-mass vibratory gyroscope with an amplitude amplification of 3.5x and a single-mass vibratory gyroscope of a comparable size and topology. This paper presents preliminary results that compare the single-mass vibratory gyroscope to the amplitude amplified dual-mass vibratory gyroscope. The dual-mass gyroscope demonstrates a better noise performance in the open-loop rate-mode with respect to its single-mass counterpart.

This material is based on work supported by the Defense Advanced Research Projects Agency and U.S. Navy under contract No. N66001-16-1-4021.

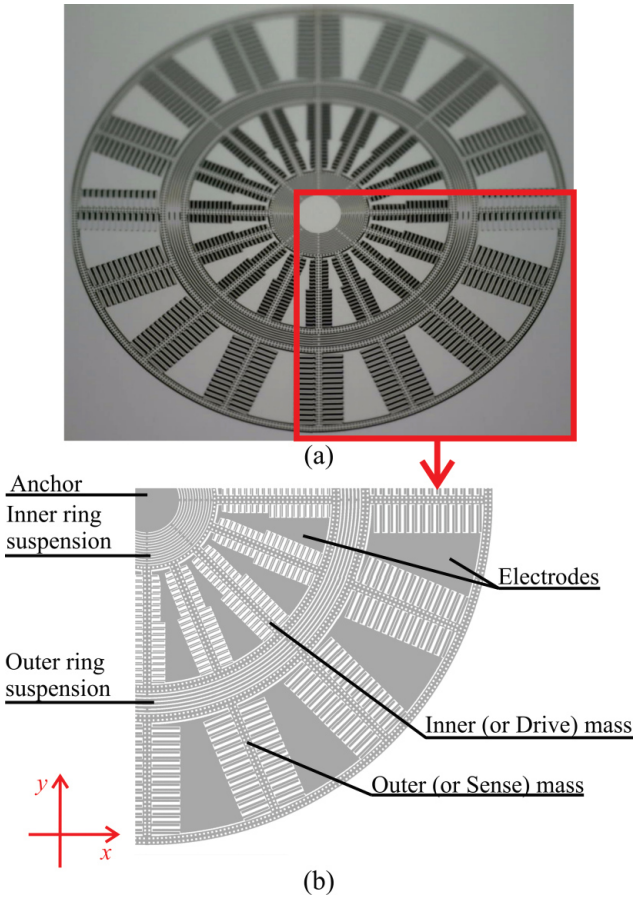

Fig. 1. (a) A dual-mass vibratory gyroscope fabricated using an in-house 100 μm SOI process; (b) Nomenclature of a close-up of the quarter of the device.

II. Dual-Mass Gyroscope Design with Amplitude Amplification

A. Dual-mass structure

The dual-mass configuration includes an inner mass, the "drive mass", attached to a central anchor and structurally coupled to an outer mass, the "sense mass", using a concentric ring suspension, Figure 1. Each mass is surrounded by 16 electrodes with parallel plates for driving, sensing, and electrostatic tuning, Figure 2. In the rate gyroscope configuration, the actuation force is applied along the x-axis of the inner

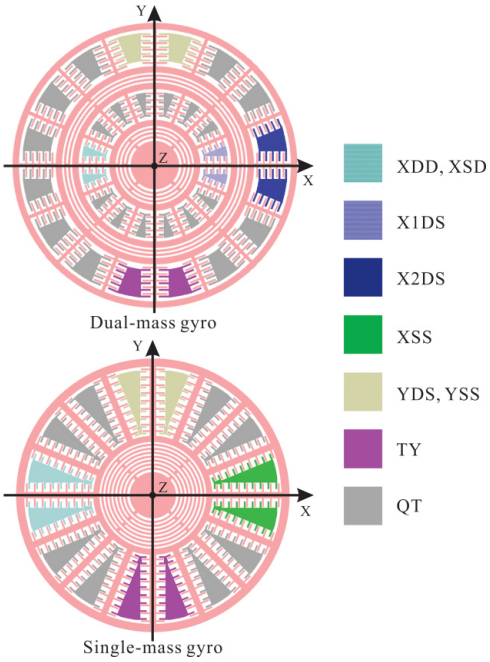

Fig. 2. Configuration of driving, sensing and tuning electrodes of the dual and single-mass gyroscopes.

mass and the Coriolis force, due to rotation along the z-axis, is detected along the y-direction of the outer mass. Adding the outer mass increases the number of degrees of freedom (DOF) of the system, and selecting the appropriate values for mass and stiffness elements enables a mechanical amplification of the amplitude of vibration.

B. Amplitude Amplification

For the dual-mass structure, the equations of motion along the drive axes (x_1 and x_2) and sense axes (y_1 and y_2) are given as [1]:

$$\ddot{x}_1 + \frac{c_1}{m_1}\dot{x}_1 + \frac{k_1+k_2}{m_1}x_1 - \frac{k_2}{m_1}x_2 = \frac{F_x}{m_1} + 2\Omega\dot{y}_1 \quad (1)$$

$$\ddot{x}_2 + \frac{c_2}{m_2}\dot{x}_2 + \frac{k_2}{m_2}x_2 = \frac{k_2}{m_2}x_1 + 2\Omega\dot{y}_2 \quad (2)$$

$$\ddot{y}_1 + \frac{c_1}{m_1}\dot{y}_1 + \frac{k_1+k_2}{m_1}y_1 - \frac{k_2}{m_1}y_2 = \frac{F_y}{m_1} - 2\Omega\dot{x}_1 \quad (3)$$

$$\ddot{y}_2 + \frac{c_2}{m_2}\dot{y}_2 + \frac{k_2}{m_2}y_2 = \frac{k_2}{m_2}y_1 - 2\Omega\dot{x}_2 \quad (4)$$

In those equations, F_x and F_y are the sinusoidal driving forces applied to the inner mass and Ω is a constant input angular rotation along the z-axis. Parameters x_1 and y_1 are displacements of the inner mass (or "drive mass") and x_2 and y_2 are displacements of the outer mass (or "sense mass"). In the primary and secondary modes, m_1 and m_2 represent the masses of the inner and outer masses, k_1 and k_2 are stiffnesses of the inner and outer ring suspensions, and c_1 and c_2 are damping coefficients associated with each mass.

The drive frequency of interest is the first resonant frequency of the dual-mass system, as depicted in Figure 3. The

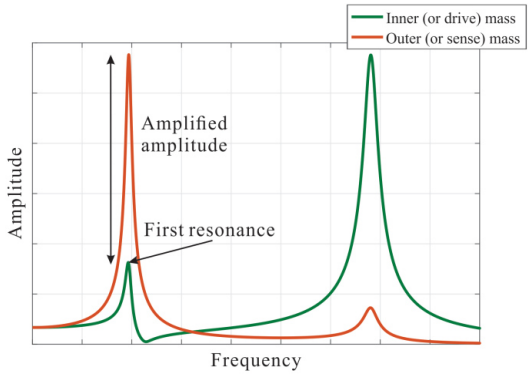

Fig. 3. Frequency response of a dual-mass architecture with amplitude amplification. By actuating the drive mass at the first resonant frequency, a large amplitude is achieved on the sense mass.

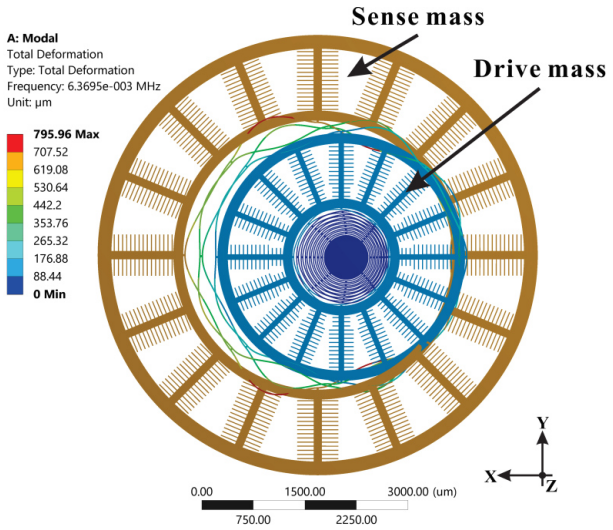

Fig. 4. FEA of a dual-mass vibratory gyroscope moving in the translational mode at 6.37 kHz, with amplitude amplification.

two resonant peaks in Figure 3 of the dual-mass system, ω_1' and ω_2', are [3]:

$$\omega_1'^2, \omega_2'^2 = \frac{1}{2}\left[\omega_1^2 + \omega_2^2 + \frac{k_2}{m_1}\right] \mp \frac{1}{2}\sqrt{\left(\omega_1^2 - \omega_2^2 + \frac{k_2}{m_1}\right)^2 + 4\frac{k_2}{m_1}\omega_2^2}, \quad (5)$$

where $\omega_1 = \sqrt{k_1/m_1}$ and $\omega_2 = \sqrt{k_2/m_2}$.

The drive mass oscillates at the first resonance frequency in response to a drive voltage provided by electrodes, and the sense mass follows the drive mass, but responds with an amplified amplitude. That means the dual-mass system operates in the translational mode with amplitude amplification at the first resonant frequency, Figure 4.

III. Rate and Rate-Integrating Gyroscopes

The single-mass and dual-mass gyroscopes can operate in both rate and rate-integrating (whole angle) measurement modes. In the rate measuring mode, an increase in the drive amplitude increases the sensitivity and reduces Mechanical-Thermal Noise (MTN). The theoretical MTN Angle Random

Walk (ARW) for gyroscopes in the open-loop operating mode is [4]:

$$ARW = \sqrt{\frac{k_B T \omega_y}{AM\omega_x^2 Q_y}\left[1+\left(\frac{Q_y(\omega_y^2-\omega_x^2)}{\omega_x\omega_y}\right)^2\right]^{-1}}, \quad (6)$$

where k_B is the Boltzmanns constant, M is the proof-mass, T is the operating temperature, A is the amplitude of drive-mode, ω_x and ω_y are the drive and sense resonant frequencies, respectively, and Q_y is the sense-mode quality factor.

In the rate-integrating mode, angular drift can be expressed as [5]:

$$\dot{\theta} \leq \frac{1}{2}\left|\Delta\left(\frac{1}{\tau}\right)\right| + \frac{q}{a}\left|\Delta\omega\right| \quad (7)$$

The angular drift is limited by anisodamping $\Delta(1/\tau)$, quadrature q, amplitude of vibration a, and frequency mismatch $\Delta\omega$. Increasing the amplitude of the gyroscope in the rate-integrating mechanization will potentially reduce the angular drift and increase the angle resolution.

The preferable structure for a whole angle gyroscopes is an isotropic oscillator which needs to be actuated by using parallel plate electrodes, [1]. As a result, the non-linear actuation and detection could limit the amplitude of the drive and sense-modes. The dual-mass amplitude amplification architecture can potentially solve the problem by achieving the full-gap detection, as the amplified amplitude in the outer (or sense) mass would be much larger than the inner (or drive) mass. In such arrangement, the drive mass will be kept at a small amplitude allowing to preserve the linearity of capacitive drive.

The gyroscopes operating in either rate or rate-integrating modes would benefit from the increased amplitude of motion. An amplitude amplified dual-mass gyroscope will result in a large and linear sense amplitude, thus a higher resolution.

Although the dual-mass vibratory gyroscope with amplified amplitude has advantages over the single-mass gyroscope, increasing the DOF of the coupled structure, from two to four, complicates the actuation and detection. The increase in DOF also presents a challenge for quadrature compensation, which needs to be simultaneously accomplished along all DOF, while preserving the amplitude amplification and a natural precession of the device in response to the Coriolis force.

IV. Comparative Study

A conventional single-mass gyroscope with a similar concentric ring suspension was used as a reference for performance comparison. Both devices were fabricated using an in-house SOI fabrication process, utilizing a 100 μm-thick silicon device layer, a 500 μm handle wafer, and a 5 μm-thick buried oxide layer between the handle and device layers.

The single-mass and dual-mass designs have a similar topology and footprint, providing a justifiable baseline for comparison. The images for each device are shown in Figure 1 and Figure 5. The gyroscopes were tested in a vacuum chamber using a similar pressure conditions (1 mTorr). The geometry, operating frequency, and drive and sense capacitances are summarized in Table I.

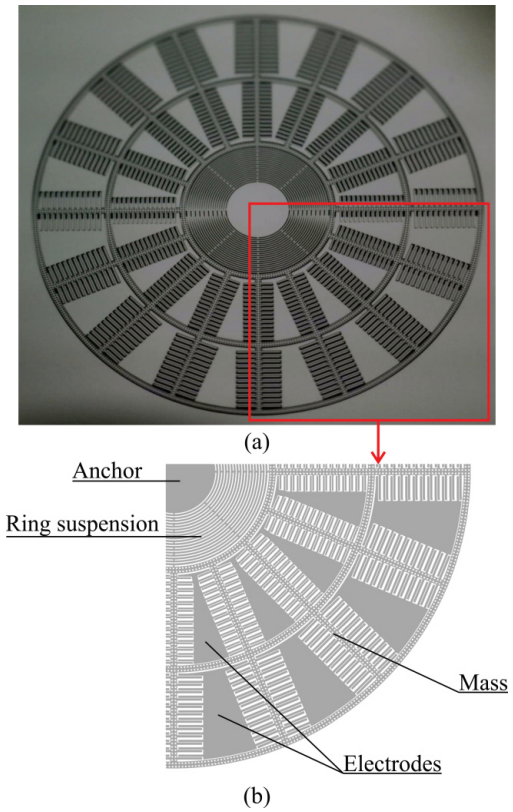

Fig. 5. (a) A single-mass vibratory gyroscope fabricated using an in-house 100 μm SOI process; (b) Nomenclature of a close-up of the quarter of the device.

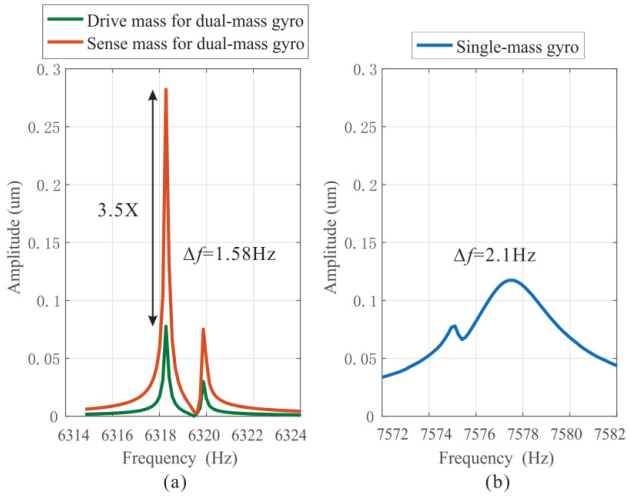

Fig. 6. Frequency response of (a) the dual-mass gyroscope with 3.5x amplified amplitude between sense and drive masses and (b) the single-mass gyroscope. The frequency mismatch of both devices is experimentally verified.

Figure 6 demonstrates the frequency responses of a single-mass and an amplitude amplified dual-mass gyroscope, when the same drive forces were applied to both devices. The condition was achieved by applying different driving voltages to the driving electrodes (XDD and XSD) of the dual and single-mass gyroscopes, compensating for their unequal drive capacitances. An amplitude amplification factor of 3.5x was experimentally measured on the dual-mass device. X1DS, X2DS, and XSS are the sensing electrodes in the x-axis. YDS and YSS are the pick-off electrodes of devices in the y-direction. The tuning voltages

TABLE I. THE SINGLE-MASS AND DUAL-MASS GYROSCOPE PARAMETERS

Gyro Type	Resonant Frequency (kHz)		Mass (kg)		Diameter	C_{drive}	C_{sense}	Tuning Voltage (V)	Freq. Mismatch after Tuning	Q
	1st peak	*2nd peak*	*Drive mass*	*Slave mass*						
Dual-mass	6.31	24.6	5.64e-7	1.23e-6	6.4mm	1.1 pF	4.26 pF	9	1.58 Hz	55k
Single-mass	7.57		3.3e-6		7.2mm	2.3 pF	3.2 pF	21	2.0 Hz	33.8k

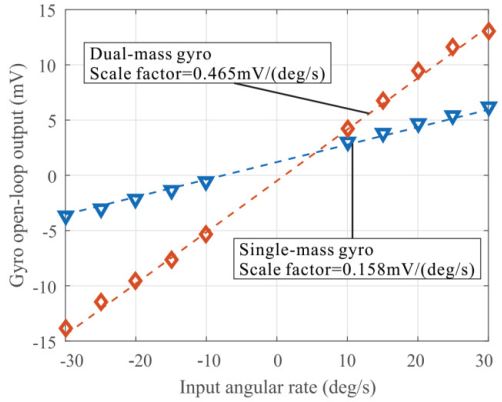

Fig. 7. Scale factors of the dual and the single-mass gyroscopes operated in the open-loop rate-mode under the same operational condition.

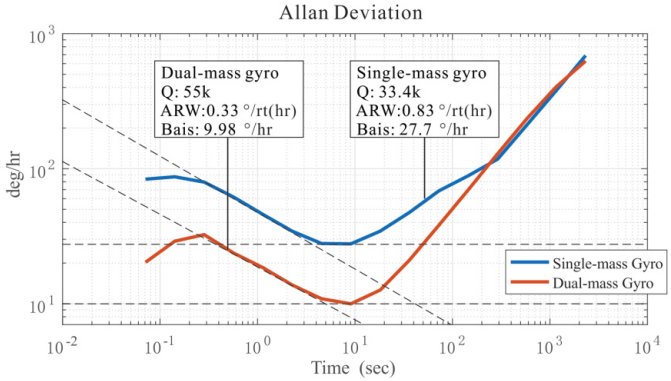

Fig. 8. The Allan Deviation of gyroscopes (tested in a vacuum chamber) in the open-loop operation mode.

and the frequency mismatch after tuning were recorded and shown in Table I. The tuning voltages for both devices were applied to the orthogonal electrodes (TY), so that the condition of the same drive forces had no effect. The QT electrodes are for quadrature tuning, but they were not used in this study.

The rate-mode characterization for the single-mass and the dual-mass gyroscopes were performed in an open-loop architecture with Phase-Locked Loop (PLL) and Amplitude Gain Control (AGC). In the dual-mass gyroscope, the AGC loop was used between the drive signal at the inner mass and the sense signal at the outer mass. The scale factors of the two devices were extracted using a rate table with the sinusoidal input rotation rates of ± 10, ± 15, ± 20, ± 25 and ± 30 (deg/s), Figure 7. The single-mass device demonstrated the scale factor of 0.158 mV/(deg/s) in the open-loop rate-mode of operation, while the dual-mass gyroscope demonstrated the scale factor of 0.465 mV/(deg/s), revealing three times the scale factor improvement in the dual-mass design as compared to the single-mass gyroscope.

All experiments were performed in the lab environment under vacuum condition without any thermal compensations. The Zero Rate Output (ZRO) experiment of the dual-mass gyroscope demonstrated a bias stability of 9.98 (deg/hr) and ARW of 0.33 (deg/rt-hr). Both bias stability and ARW resulted in a better performance as compared to the single-mass gyroscope, with measured 27.7 deg/hr bias stability and 0.83 deg/rt-hr ARW. The Allen Deviation plots are shown in Figure 8, demonstrating a better noise characteristic of the amplitude amplified dual-mass gyroscope. As expected, the scale factor and bias stability of the MEMS gyroscopes improves as the sense amplitude increases, due to the amplitude amplification architecture.

V. CONCLUSION

We experimentally demonstrated the amplitude amplification concept in a dual-mass MEMS gyroscope architecture. A comparative study of the single-mass and dual-mass devices has been reported in this paper. The comparative experiments suggested that the dual-mass vibratory gyroscopes with the amplitude amplification possesses a larger scale factor, 0.465 mV/(deg/s) versus 0.158 mV/(deg/s) for the single-mass without amplitude amplification, and higher in-run bias stability of 9.98 deg/hr and ARW of 0.33 deg/rt-hr, as compared to the single-mass gyroscope, with measured 27.7 deg/hr bias stability and 0.83 deg/rt-hr ARW. The dual and single-mass devices were of a comparable footprint. These preliminary results demonstrated some potential advantages of the dual-mass gyroscope with amplitude amplification over the conventional MEMS gyroscope, without amplitude amplification.

ACKNOWLEDGMENTS

The MEMS gyroscopes were designed and characterized at UCI Microsystems Laboratory. Devices were fabricated at UCI INRF cleanroom facility.

REFERENCES

[1] A. M. Shkel, "Type I and type II micromachined vibratory gyroscopes," in *IEEE/ION PLANS*, San Diego, CA, USA, April 25-27, 2006.

[2] C. C. Painter and A. M. Shkel, "Dynamically amplified micromachined rate intergrating gyroscope," in *Intern. Conf. On Modeling and Simulation of Microsystems (MSM2003)*, San Francisco, CA, USA, February 23-27, 2003.

[3] C. Painter and A. Shkel, "Dynamically amplified rate integrating gyroscopes," Aug. 16 2005. US Patent 6,928,874.

[4] R. P. Leland, "Mechanical-thermal noise in MEMS gyroscopes," *IEEE Sensors Journal*, vol. 5, no. 3, pp. 493–500, 2005.

[5] D. D. Lynch, "Vibratory gyro analysis by the method of averaging," in *Proc. 2nd St. Petersburg Conf. on Gyroscopic Technology and Navigation; St. Petersburg, Russia*, vol. 1, pp. 26–34, 1995.